DEPARTMENT OF DEFENCE
DEFENCE SCIENCE & TECHNOLOGY ORGANISATION
DSTO

An Experimental and Numerical Study of IR Emission from a Porous Radiant Burner

Farid C. Christo and
Lakshmanan V. Krishnamoorthy

DSTO-TR-1154

An Experimental and Numerical Study of Infrared (IR) Emission from a Porous Radiant Burner

Farid C. Christo and Lakshmanan V. Krishnamoorthy

Weapons Systems Division
Aeronautical and Maritime Research Laboratory

DSTO-TR-1154

ABSTRACT

An experimental analysis and computational modelling of thermal radiation from an INCONEL601 wire-mesh porous burner has been conducted. It has been found that within a bandwidth between 2μm and 20μm, the infrared radiation in the 2-5μm waveband is the dominant band. Optimal operating conditions, as determined by the surface temperature and radiant intensity, are a function of the equivalence ratio and the firing rate. The location of the flame front is also influenced by these parameters. For fuel-rich mixtures the flame is usually located above the surface and the flame stability is sensitive to external perturbations. A maximum surface temperature of approximately 1223K, and a radiation intensity of 50 W/Sr, has been measured. It has also been shown that INCONEL601, despite its high emissivity, can be used as an effective radiation shield. By placing a piece of the wire-mesh in front of burning MTV pyrotechnic composition, the infrared radiation was significantly reduced. The equivalent black body temperature of MTV was cut from ~1900°C without a shield to ~1400°C with a shield adjacent to the mixture.

A comparison between the ChemRad model predictions and measured surface temperature for various equivalence ratios has shown a reasonable agreement with a maximum discrepancy of 16% for fuel-rich mixtures. However, within optimal operating conditions of the burner (equivalence ratio 0.8- 1) a maximum difference of 8% has been observed. Accounting for the variability in the measurements, the number of simplifying assumptions and the uncertainty in some values of the physical and optical properties, the accuracy and consistency of the model, as a first-order approximation is acceptable.

Published by

DSTO Aeronautical and Maritime Research Laboratory
506 Lorimer St
Fishermans Bend Vic 3207 Australia

Telephone: (03) 9626 7000
Fax: (03) 9626 7999

AR-011-870
May 2001

APPROVED FOR PUBLIC RELEASE

An Experimental and Numerical Study of Infrared (IR) Emission from a Porous Radiant Burner

Executive Summary

The work presented in this report is aimed at investigating the infrared intensity emitted from an INCONEL601 wire-mesh porous burner, and validating the numerical ChemRad model. Thermal radiation within 2-20 μm waveband has shown that the dominant radiation energy (~65%) is concentrated within the 2-5μm waveband. Within this region only spectra of CO_2 and H_2O have been observed. It has been found that optimal operating condition of a porous burner is influenced by the fuel-to-air ratio as well as the firing rate. These parameters also affect the flame front location and the stability of the flame. For fuel-rich mixtures the flame is located above the surface of the burner, while for fuel-lean and stoichiometric mixtures the flame is either embedded within the porous layer or located close to the surface. The latter cases correspond usually to a radiant mode of operation. On average, a surface temperature of approximately 1223K and radiant intensity between 30 W/Sr and 60 W/Sr (in the 2-5μm waveband), have been measured at stoichiometric propane-air mixture operating at firing rates between 130 kW/m^2 and 400 kW/m^2. These measured radiant intensity (30-60 W/Sr) however, are considered too low for application as air decoy or tracking flares (which typically require intensity in the order of kilowatts per steradian).

The most useful property of the INCONEL601 wire-mesh, which was discovered accidentally, is its effectiveness as a radiation shield. By placing a piece of INCONEL601 close to an Magnesium/Teflon-based compositions (MTV) specimen, the radiant intensity of the burning of MTV mixture was reduced significantly. The equivalent black body temperature of MTV of approximately 2170K has been reduced to 1670K when the INCONEL601 wire-mesh is placed adjacent to the MTV specimen and the radiation intensity is reduced by a factor of four. This result implies that the INCONEL601 has a potential use as a radiation shield to mask or alter the IR signature of naval and land platforms.

The measured surface temperature has been used to validate the predictions of the numerical model, ChemRad. Overall, a reasonable agreement between the model and the measurements has been found, especially for fuel-lean and stoichiometric mixtures, with a maximum relative error of 8%. However, for fuel-rich mixtures, larger errors of up to 16% have been recorded. Considering the variability in the measured results, the simplifying assumptions and the uncertainty in the values of some of the physical and optical properties used in the model the accuracy and consistency of the model as a first order approximation, is acceptable.

Authors

Farid C. Christo
Weapons Systems Division

Farid Christo holds a B.Sc.(1986) and M.Sc. (1989) in Aeronautical Engineering. His main expertise are combustion, CFD, thermo-fluids and propulsion systems. Between 1990 and 1993 he worked at the University of Sydney on a joint project with Pacific Power Corporation. His work focused on the development and validation of computer models to predict the flow field and erosion rate of heat recovery tubes in boilers of coal-fired power stations. In 1996, he gained his PhD. from the University of Sydney, Department of Mechanical and Mechatronic Engineering. His research topic was the development of artificial neural networks for applications in turbulent combustion simulations. He then joined the Sydney-based company Biomass Energy Services and Technology, where he worked on modelling industrial aerodynamics and combustion processes. In April 1998 he joined the DSTO as a Research Scientist with Weapons Systems Division, Salisbury. Farid's current research interest is the development of computational capabilities for modelling aerothermochemical processes of pyrotechnics and advanced propulsion systems.

Lakshmanan V. Krishnamoorthy
Weapons Systems Division

Lakshmanan Krishnamoorthy graduated from the Indian Institute of Science, Bangalore, India, with ME in Aeronautical Engineering. Between 1977 and 1982, he worked as an aero engineer in Helicopter Design Bureau at Hindustan Aeronautics Ltd, Bangalore, India. He gained his PhD in 1988, in Mechanical Engineering from the University of Newcastle, NSW. Subsequently he worked as post-doctoral research assistant at the Imperial College of Science & Technology, UK and the University of Sydney. He joined WSRL, DSTO Salisbury in 1991 and has been working in the field of exterior ballistics. His current interests are in modelling IR Countermeasure systems.

Contents

1. INTRODUCTION 1

2. EXPERIMENTAL FACILITY 1
2.1 Burner Design and Set-up 1
2.2 Controls and Instrumentations 4
2.2.1 MERLIN Radiometers 4
2.2.2 BOMEM MR-254 Fourier Transform (FT) spectrometer 4
2.2.3 AGEMA Thermovision 900 thermal-imaging system 4
2.2.4 MIKRON Pyrometer 5
2.2.5 FLUKE Thermocouple 5

3. THE NUMERICAL MODEL 5

4. EXPERIMENTAL AND NUMERICAL PARAMETERS 6
4.1 Experimental Parameters 6
4.2 Numerical Parameters 6

5. RESULTS AND DISCUSSION 7
5.1 Experimental Results 7
5.1.1 Temperature and Radiation Intensity Measurements 7
5.1.2 Thermal Imaging Results 11
5.1.3 Spectral IR Measurements 15
5.2 Numerical Results 17
5.3 Comparison Between Predictions and Experiment 23
5.4 INCONEL601 as a Radiation Shield 25

6. CONCLUDING REMARKS 27

7. ACKNOWLEDGMENTS 27

8. REFERENCES 28

APPENDIX A:CALIBRATION AND ANALYSIS FOR BOMEM MR254 SPECTROMETER 29

APPENDIX B: CALIBRATION AND ANALYSIS METHODOLOGY FOR THERMAL IMAGER DATA 31

1. Introduction

The wide use of pyrotechnics formulations of Magnesium/Teflon-based compositions as infrared (IR) decoy flares stems from their large energy output. When ignited, they burn with an anaerobic combustion zone, followed by an intense mixing region where the hot combustion products yield their thermal energy via mixing, secondary combustion with atmospheric air resulting in intense radiation. At high air speeds, the heat loss is dominated by atmospheric mixing whereas under low speeds, the heat loss is primarily through radiation. The combustion process of flares is similar to conventional premixed flames, where heat conduction is the dominant mode of heat transfer. Improvements to the heat transfer characteristics, especially thermal radiation mechanism in premixed flames can be achieved using Porous Radiant Burners (PRBs) technology. PRBs are manufactured either from ceramic or stainless steel fibres or from fired clay. A premixed gas and air are forced to flow into the ceramic and burn just on or under the surface, transferring heat to the solid from the flame. The heat transfer is dominated by radiation. The development of PRBs was initially driven by the need to improve thermal efficiency of existing heat generating facilities and also to provide lower emissions of hazardous gases by complete combustion.

It is proposed that the PRB technology be examined as a potential candidate for defence applications. More specifically, investigating the spectral emission and total power density of PRBs to determine their suitability for countermeasure or tracking applications. To the best knowledge of the authors no such utilisation has been attempted. The prime objectives of the present study are firstly to investigate the spatially and spectrally resolved information of the emitted thermal radiation from PRBs. Secondly to use the measurements to validate the ChemRad numerical model that has been described in an earlier study[1].

PRB design, set-up and instrumentations are discussed in section 2. The numerical model describing the PRB combustion is introduced in section 3, and the experimental and numerical parameters are given in section 4. The experimental and numerical results are detailed in section 5.

This study was conducted under an AIR-sponsored task, 98/116, Pyrotechnic Infrared Countermeasures for RAAF.

2. Experimental Facility

2.1 Burner Design and Set-up

Two wire-mesh burners have been designed and manufactured. One burner, shown in Figure 1 (left), has a cylindrical geometry that is similar to in-service flares. The burner is 40 mm in diameter and 135 mm in length. However, only half of the cylinder surface is used, creating a burning surface area of 82 cm^2. The second burner, shown on the right of Figure 1, has a rectangular edge of 160 mm x 160 mm. The flatbed burner is 15 mm concaved outward at the centre creating an effective surface area of approximately 270 cm^2. This induced curvature is designed to reduce thermal stresses that could lead

to mechanical failure of the wire. Using flatbed geometry allows the effects of surface area and burner shape on flame stability and IR emission intensity to be examined.

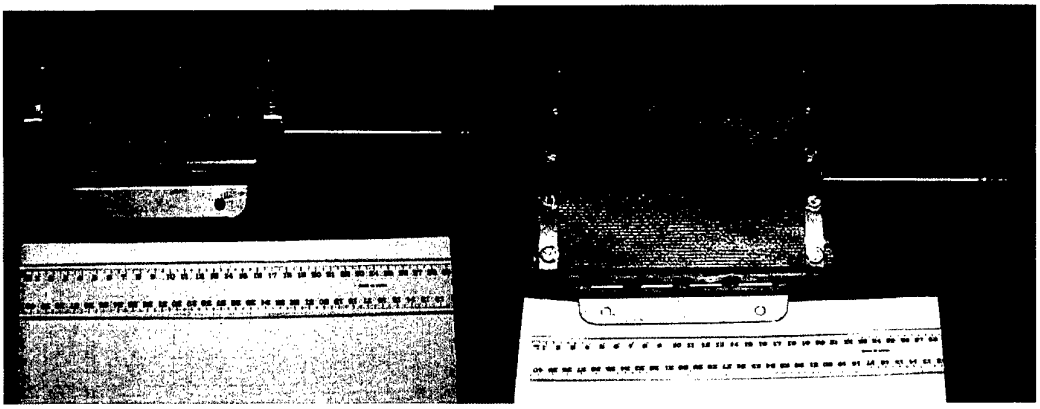

Figure 1: Close-up photographs of semi-cylindrical wire-mesh (left) and flatbed (right) burners.

Both burners use a commercial INCONEL601 wire-mesh. Three layers of mesh have been combined creating a porous medium of a 3 mm effective thickness. INCONEL601 is a nickel-chromium-iron alloy (80%-Ni, 16%-Cr, and 7%-Fe) that has excellent mechanical properties. It is also resistant to oxidation in air for up to ~1100°C. The mesh's woven pattern and induced curvature enhances flame stability, improves the mechanical strength of the lattice and reduces wrangling of the mesh due to thermal stresses. A magnified close-up photograph of the wire pattern is shown in Figure 2.

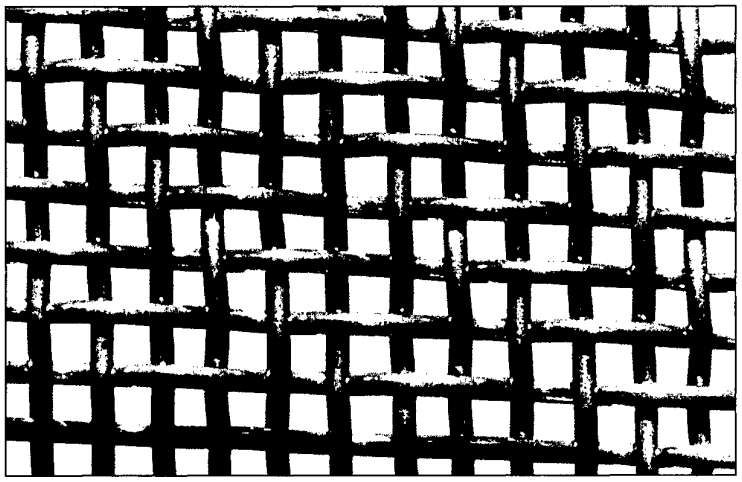

Figure 2: A photograph (X10) of an INCONEL601 wire-mesh.

A commercial liquefied petroleum gas (LPG) fuel is mixed with compressed air before entering the settling chamber of the burner, as shown schematically in Figure 3. To ensure a uniform supply of the fuel-air mixture across the entire surface of the burner and to reduce the possibility of flame flashback, a layer of stainless steel wire-mesh has been inserted in the settling chamber. An external flashback arrester has also been fitted to the fuel line as shown in Figure 4, which shows the flatbed burner in

operation, while Figure 5, shows the (visual) difference between a PRB flame and a conventional blue-flame.

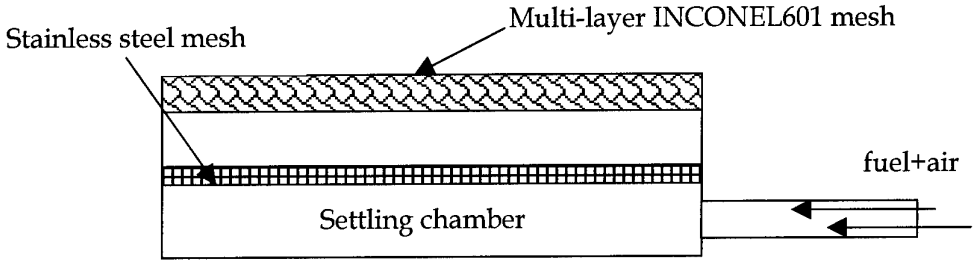

Figure 3: A schematic description of the components of the wire-mesh porous burner.

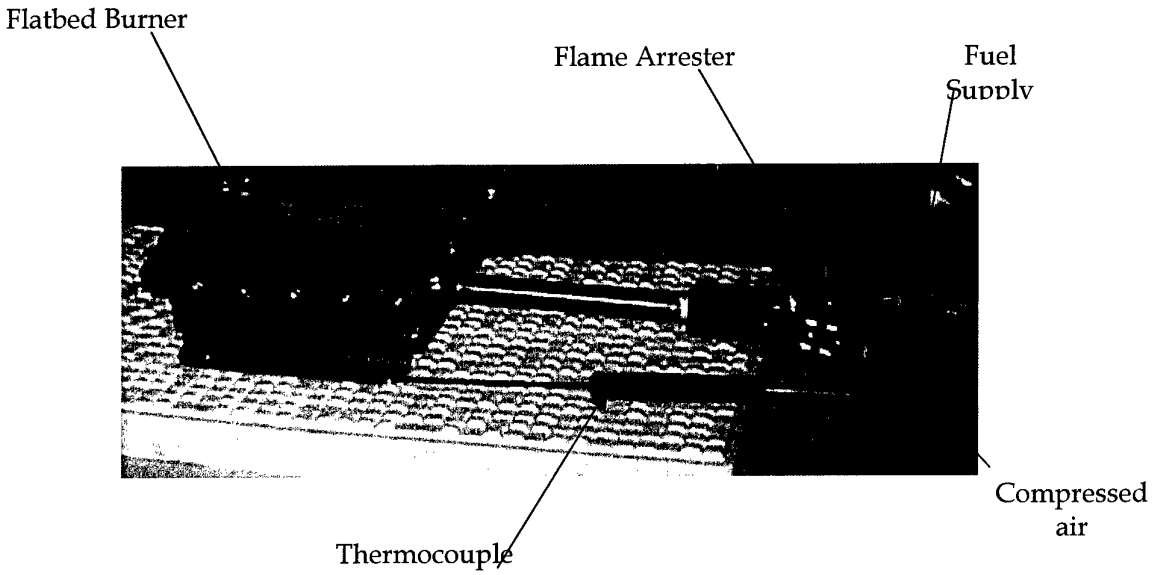

Figure 4: A photograph of the burner's supply fuel and air streams.

Figure 5: A close-up photograph of Sydney University's 'blue-flame' burner (left) and DSTO's Porous Radiant Burner (right).

2.2 Controls and Instrumentations

An instrumentation board was used to monitor and control the supply pressure, temperature and flow rates of the fuel and the air streams. An Operating Instruction addressing safety issues, ignition and shutdown procedures has also been written[2]. A number of instruments have been used to measure the gas and surface temperatures and radiation intensity. The layout of the instruments shown in Figure 6, have been located approximately 3 meters away form the burner, included:

(I) A MERLIN radiometer ,
(II) A BOMEM MR-254 Fourier Transform (FT) spectrometer,
(III) An AGEMA Thermovision 900 thermal-imaging system,
(IV) A MIKRON M90 single-colour IR Pyrometer , and
(V) A FLUKE K-Type thermocouple.

2.2.1 MERLIN Radiometers

A MERLIN radiometer employing Indium Antiminide (InSb) detector, configured for nominal spectral band of 3-5μm, was used to measure radiant intensity. Laboratory calibrations of the radiometer were performed before the experiments using the blackbody furnace operated at 1273K for various aperture diameters and stand off distances. The apparent radiant intensity was obtained using a blackbody at 720 K as the normalised target spectrum.

2.2.2 BOMEM MR-254 Fourier Transform (FT) spectrometer

The BOMEM FT spectrometer is a dual band system with an InSb detector measuring in 1800-5000cm^{-1} (2-5.5 μm) spectral region and a Mercury Cadmium Telluride (MCT) detector measuring in the 500-5000 cm^{-1} (2-20 μm) region. It produces spectrum with a 4 cm^{-1} resolution at a scan rate of 31 Hz. On site calibration of the spectrometer was performed using a blackbody furnace. Calibration to radiance values was performed using a two-temperature blackbody technique as outlined in Appendix A.

2.2.3 AGEMA Thermovision 900 thermal-imaging system

The AGEMA thermal imager has a dual scanner configured with nominal 3-5 μm and 8-12 μm spectral bands and has lenses to provide 10°HX5°V Field Of View (FOV). The 3-5 μm scanner used two InSb serial detectors while the 8-12 μm scanner used a single MCT detector. The thermal imager calibration and analysis methodologies are described in Appendix B. The pixel digital values (V) are converted to temperature (T) using the following equation

$$V = \frac{R}{\exp(B/T) - F}$$

where R, B and F are constants obtained through calibration. The AGEMA provides a two-dimensional mapping of surface temperature as well as that of the hot combustion gases around the burner. This mapping also provides information about the uniformity

of the flow field around the burner, so effects of external disturbances on surface temperature and flame stability can be identified.

2.2.4 MIKRON Pyrometer

A MIKRON-M90 single-colour infrared pyrometer was used to measure the temperature, at a point-location, on the burner's surface. It has a temperature range of 250°C - 2000°C and a spectral response between 1.0μm and 1.6μm. The emissivity of the surface should been known and properly set to ensure accurate results.

2.2.5 FLUKE Thermocouple

A FLUKE K-Type (Chromel-Alumel) thermocouple has been attached externally to the housing of the burner. The thermocouple has a temperature range between -200°C and 1370°C with a resolution of ±0.1% of the reading +0.7°C. It is used as a safety measure to monitor the temperature of the mixture in the settling chamber. If the chamber's temperature (due to heat transfer from the flame zone) is close to the auto-ignition temperature of the fuel-air mixture, the system should then be shutdown.

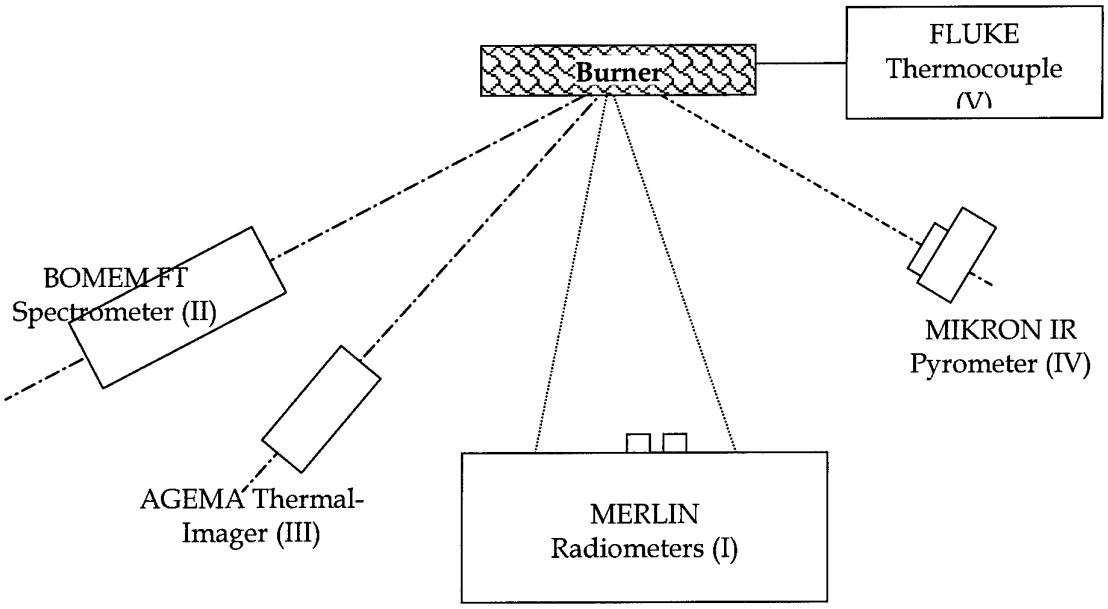

Figure 6: Layout of the instrumentations used in the experiment.

3. The Numerical Model

The ChemRad model[1] has been used to simulate the combustion and radiation processes. Calculations are carried out for propane/air mixtures with various fuel-to-air ratios and firing rates similar to those used in the experiment. The computational domain, shown in Figure 7, comprises an inlet section, a porous medium section and an exit section. For simplicity the inlet section was not considered. That is, it is assumed that $x_{in} = x_0 = 0$, while x_L is set to 0.3 cm, and x_{out} is selected to be 1 cm.

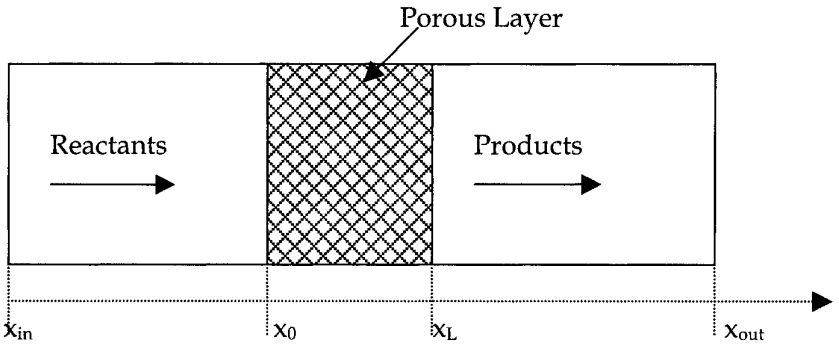

Figure 7: A schematic of the computational domain - ChemRad model.

4. Experimental and Numerical Parameters

4.1 Experimental Parameters

The equivalence ratio ϕ_c, is used to characterise the fuel/air mixtures. It is defined as the fuel-to-air ratio (FAR) on mass basis to its stoichiometric ratio (FAR_s) :

$$\phi_c = \frac{FAR}{FAR_s} .$$

The equivalence ratio can also be simply be described in terms of a global chemistry of a propane-air mixture as:

$$\phi_c C_3H_8 + 5(O_2 + 3.76N_2) \rightarrow \text{Products}$$

The flow rate of the fuel is used to characterise the firing rate (power density) of the burner, which is defined as the thermal power input per unit surface area of the burner.

4.2 Numerical Parameters

The chemistry of LPG has been represented using a high-temperature propane kinetics mechanism with 40 reactive species and 93 elementary reactions[1]. The model-input parameters, ie. optical and physical properties of the porous medium that are used in the calculations are listed in Table 1. Optical properties are often difficult to obtain experimentally or analytically, and even documented values in the literature retain a certain degree of uncertainty. Furthermore, some optical properties also depend on the microstructure of the porous. That is the manufacturing techniques used for preparing the material could have a profound influence on its optical properties [3].

Table 1: A list of optical properties of INCONEL601 used in the calculations.

Parameter	Physical units	Value	Note [Uncertainty]
Void	-	0.95	Estimated [low]
Tortuosity	-	3.36	Estimated [medium]
Area Density	cm^2/cm^3	44	Estimated [high]
Emissivity	-	0.8	Manufacturer specs [low]
Reflectivity	-	0.9	Literature [medium]
Albedo	-	0.7	analysis Parametric [high]
Extinction coefficient	cm^{-1}	50	Parametric analysis [high]
Forward scattering	-	0.5	Parametric analysis [high]
Backward scattering	-	0.5	Parametric analysis [high]

5. Results and Discussion

First, the results of the experiment are presented followed by analysis of code predictions. A comparison between the numerical and the measurements is then presented and the capabilities of the numerical model are commented upon.

5.1 Experimental Results

Two sets of experiments have been conducted, one using the semi-cylindrical burner and another for the flatbed burner. In each experiment the surface temperature of the burner, the apparent radiation emission in the 3-5 μm waveband and the spectral emission have been measured. Measurements have been carried out for different fuel-to-air ratios, ϕ_c ranging from 0.3 to 1.5. The stoichiometry of the mixture was adjusted by changing the airflow rate, keeping the fuel flow rate (which determined the firing rate of the burner) unchanged. In this study firing rates between 139 kW/m^2 and 417 kW/m^2, have been achieved. Using different firing rates allows the optimal the operating condition of the burner, both in terms of flame stability radiative output to be achieved. It is worth mentioning that for industrial applications a firing rate of 400 kW/m^2 is considered moderate. However, for feasibility and exploratory purposes a higher firing rate is not necessary as long as the flame is stable and the measurement resolution is adequate.

5.1.1 Temperature and Radiation Intensity Measurements

Tables 2 and 3 summarise the measured surface temperature and radiant intensity for the semi-cylindrical and the flatbed burners. The surface temperature (T_s) has been measured by the MIKRON IR-pyrometer and the apparent radiation in the 3-5 μm waveband (Q^{3-5}) has been measured using the MERLIN radiometers. The results are also presented in Figures 8-11.

Figure 8 shows the surface temperature of the semi-cylindrical burner for various equivalence ratios and firing rates. A maximum surface temperature of 1205K has been measured at firing rate of 417 kW/m^2. Surface temperatures of 1069K and 1162K have been recorded at firing rates of 139 kW/m^2 and 278 kW/m^2, respectively. However, the

peak-temperature location (in ϕ_c space) exhibits a dependency on the firing rate, shifting towards the stoichiometric ratio as the firing rate increases. Similar behaviour has also been observed for the flatbed burner, as shown in Figure 9. Similar behaviour has also been observed for the flatbed burner. The results presented in Figures 8 and 9, indicate that unlike blue-flame burners, the highest surface temperature in a PRB does not always occur at a stoichiometric mixture, as both equivalence ratio as well as the firing rate influences the optimal operating conditions of a PRB.

Table 2: Experimental results for the semi-cylindrical burner. Key: P_I = Power input, P_D = Firing Rate, ϕ_c = equivalence ratio, T_s= Surface temperature as measured by IR-Pyrometer, $Q_r^{3\text{-}5}$= Apparent radiation in 3-5 μm waveband as measured by the MERLIN radiometers.

Exp. ID	P_I (kW)	P_D (kW/m²)	ϕ_c	T_s (K)	$Q^{3\text{-}5}{}_R$ (W/sr)
C1A	1.14	139	0.58	1087	45.24
C2A			0.43	1112	31.14
C3A			0.39	1069	32.01
C4A			0.35	1026	29.98
C5A			0.31	810	27.37
C6A	2.27	278	0.53	938	18.38
C7A			0.581	1080	27.60
C8A			0.63	1115	36.30
C9A			0.70	1141	38.97
C10A			0.77	1162	42.05
C11A			0.87	1043	44.37
C12A			1.00	1043	43.26
C13A			1.16	915	41.47
C14A			1.40	783	39.78
C15A	3.41	417	1.75	726	35.78
C16A			1.50	730	43.79
C17A			1.31	865	46.05
C18A			1.16	1003	47.21
C19A			1.05	1122	51.21
C20A			0.95	1205	56.43
C21A			0.87	1190	57.65
C22A			0.80	1032	57.65

Table 3: Experimental results for the flat-bed burner. Key: P_I = Power input, P_D = Firing Rate, ϕ_c = equivalence ratio, T_s= Surface temperature as measured by IR-Pyrometer, Q_r^{3-5}= Apparent radiation in 3-5 μm waveband as measured by the radiometer.

Exp. ID	P_I (kW)	P_D (kW/m²)	ϕ_c	T_s (K)	Q^{3-5}_R (W/sr)
F1A	1.70	63	1.05	875	20.126
F2A			0.87	961	23.548
F3A			0.65	973	21.808
F4A			0.52	953	19.836
F5A			0.43	873	18.908
F6A			0.41	658	15.428
F7A	3.41	126	0.80	1075	8.874
F8A			0.87	1101	35.728
F9A			1.05	1021	42.688
F10A			1.31	907	44.254
F11A			1.75	803	45.994

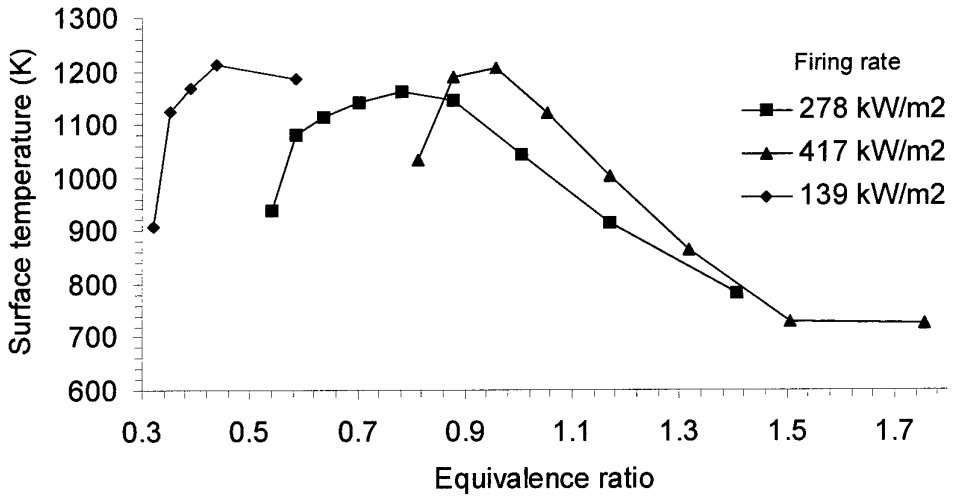

Figure 8: Measured surface temperature of the porous burner for various equivalence ratios and different firing rates(semi-cylindrical burner).

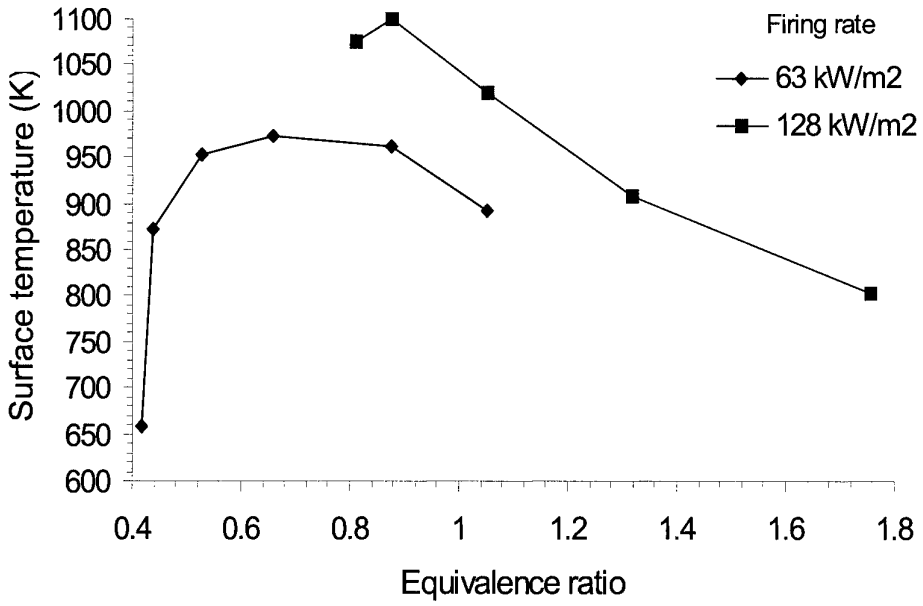

Figure 9 : Measured surface temperature of the porous burner for various equivalence ratios and for different firing rates(flatbed burner).

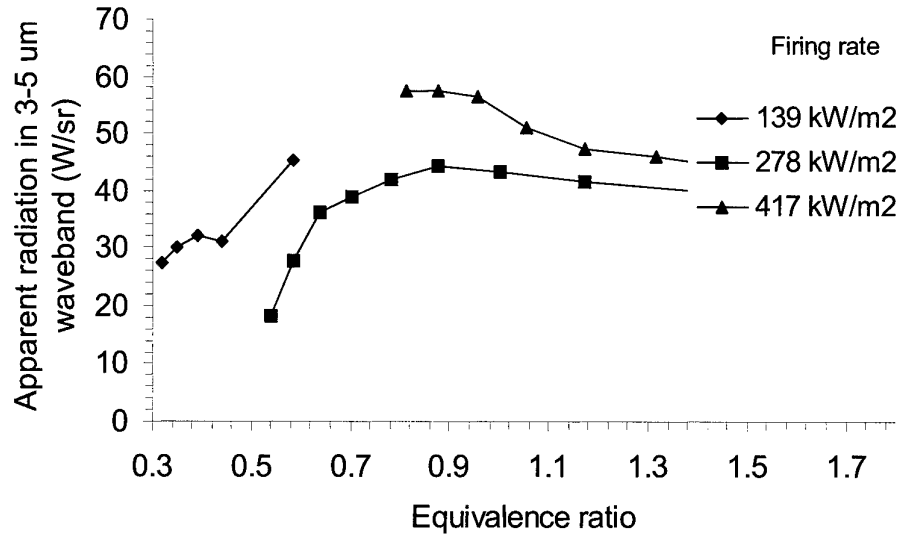

Figure 10: Apparent radiation in 3-5 micrometer waveband at various equivalence ratios and different firing rates(semi-cylindrical burner).

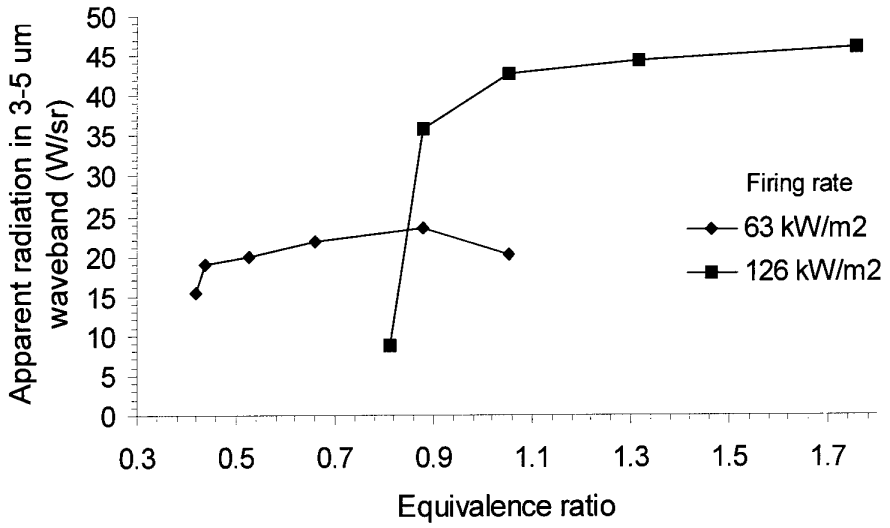

Figure 11: Apparent radiation in 3-5 micrometer waveband at various equivalence ratios and different firing rates(flat-bed burner).

Figures 10 and 11 show the apparent radiation intensity in 3-5 μm waveband for the semi- cylindrical and the flatbed burners, respectively. As shown, increasing the firing rate leads to a noticeable increase in the maximum apparent radiation, especially for the flatbed burner. The effect of the equivalence ratio on the magnitude and location of peak radiation intensity, however, is less pronounced with only small variations in intensity over a wide range of equivalence ratios.

The results shown in Figures 8-11 also highlight PRB's ability to maintain a stable combustion over a broader range of fuel-to-air ratios than blue-flame burners [4,5]. The lower and upper flammability limits of a propane-air mixture burning in a conventional burner are 0.5 and 1.6, respectively. These limits however are extended to 0.3 and 1.7, respectively for the same mixture burning in a porous burner.

5.1.2 Thermal Imaging Results

The AGEMA system has been used to measure and visualise the spatial distribution of temperature at the surface and the surrounding of the burner. It also provides information about the uniformity (or lack of it) in the temperature and flow fields around the burner. Figure 12, shows temperature contours from the semi-cylindrical burner operating at stoichiometry (ϕ_c=1) and firing rates of 278 kW/m^2, and 417 kW/m^2. Similarly, Figure 13, shows temperature contours from the flatbed burner operating at stoichiometry and firing rates of 63 kW/m^2, and 126 kW/m^2.

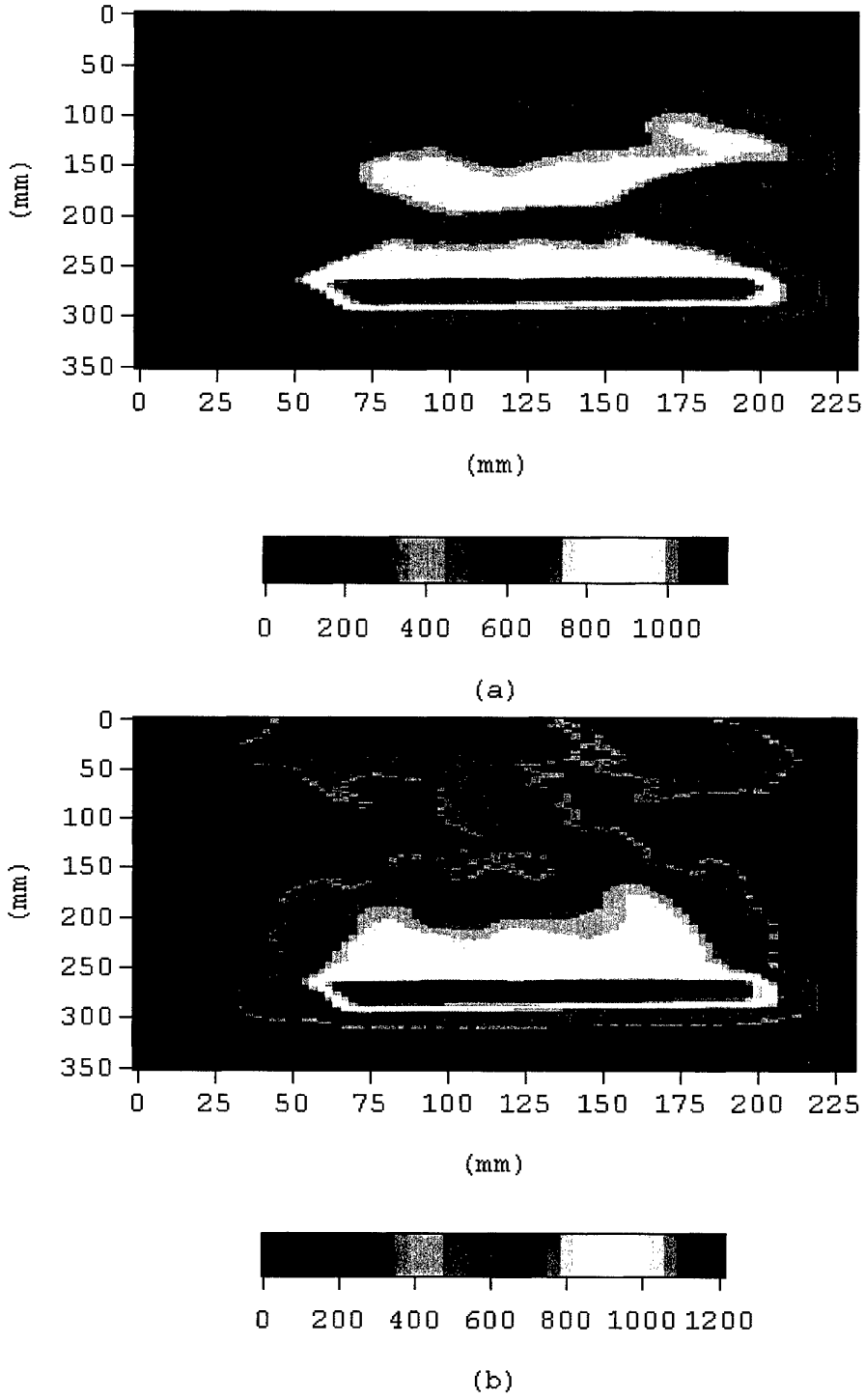

Figure 12: AGEMA's temperature contours(°C) for the semi-cylindrical burner operating at a power density of (a) 278 kW/m², (b) 417 kW/m² (a stoichiometric propane-air mixture).

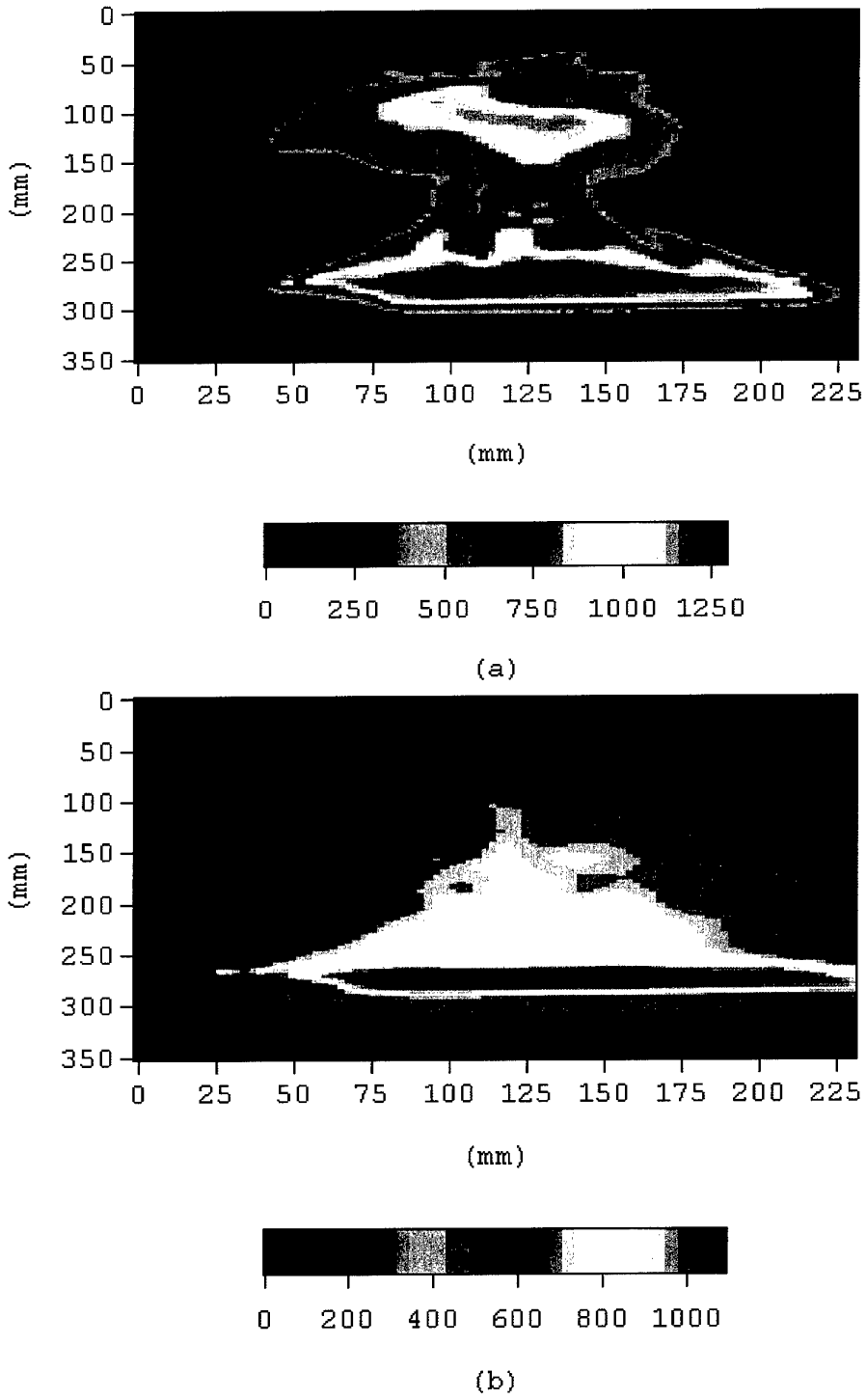

Figure 13: AGEMA's temperature contours (°C) from the flat-bed burner operating at a power density of (a) 63 kW/m², (b) 126 kW/m² (a stoichiometric propane-air mixture).

As shown in Figure 12, the temperature distribution is reasonably uniform around the semi-cylindrical burner, up to a (vertical) distance of about 50 mm above the surface of the burner. The temperature distribution along the lateral direction also shows very

little variations. The temperature field for the flatbed burner (Figure 13) however, is less uniform in the downstream direction, particularly at low firing rate of 63 kW/m^2 where portion of the flame seems to lift-off from the surface. It is worth noting that at this firing rate the burner was not operating in a radiant mode. As the firing rate and the equivalence ratio are adjusted to an optimal level (which is burner-specific) the flame tends to change to a radiant mode with a red-glowing surface. Further increase in the equivalence ratio or the firing rate however, tends to lift-off the flame from the surface and subsequently the flame blows-off completely. In this series of experiments the burners were not shielded. However the results indicate that air movement in the laboratory has little effect on the uniformity of the temperature and flow fields above the burner. As our interest in focused on measuring surface and gas temperature up to 20 mm from the surface, the uniformity of flow and temperature in the near field is considered adequate.

Using the AGEMA's temperature readings, mean axial temperature profiles of the hot gases have been extracted as follows. At each axial location, the average temperature (and its r.m.s.) is calculated using 21 temperature readings (along the lateral direction). Figure 14, shows the mean and standard deviation of the gas temperature, up to 12 mm from the surface of the semi-cylindrical burner (417 kW/m^2) and for a range of equivalence ratios (ϕ_c = 0.8 - 1.75). The small standard deviation indicates that the temperature along the lateral direction of the burner is reasonably uniform. It can also be seen that the gas temperature decays rapidly within a short distance from the surface. For equivalence ratios between 0.8 and 1.3, the gas temperature drops from the surface temperature to a temperature of 600°C- 700°C, within 12 mm from the surface of the burner.

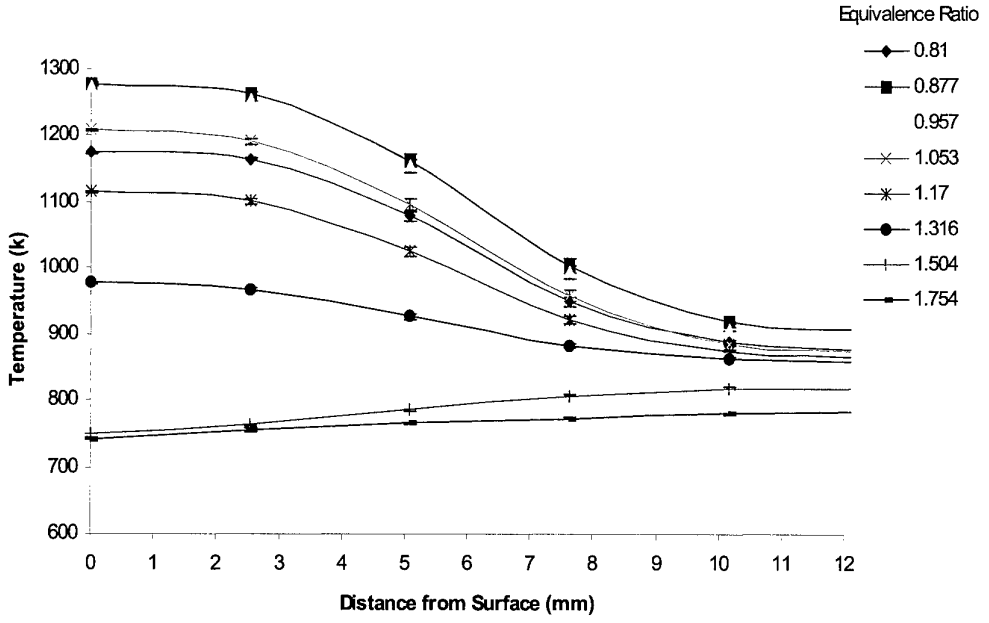

Figure 14: Axial mean and standard deviation of gas temperature of the semi- cylindrical burner operating at 417 kW/m^2, over a broad range of equivalence ratios.

5.1.3 Spectral IR Measurements

Figure 15 shows a spectral IR emission for five different mixtures, as measured using the BOMEM broad band detector in a 2-20 μm waveband. It clearly shows that the bulk of the energy is concentrated primarily within the 2-5μm region. More specifically approximately 65% of the total energy is concentrated within the 2-5 μm waveband. Furthermore within the 2-5 μm waveband the energy on average is distributed approximately as 25% within 2-3 μm, 15% within the 3-4 μm, and 60% within the 4-5 μm waveband. This pattern has also been observed for other mixtures and power densities. Therefore all subsequent measurements are collected using a detector with a narrower bandwidth of 2-5 μm. Figure 16, shows the IR intensity within the 2-5 μm waveband for different mixtures and firing rates. In all cases, the peak IR emission occurs at approximately 4.38 μm, which corresponds to a strong band of radiation from CO_2 molecules. It is interesting to notice that whilst CO has a strong band at 4.7μm, and a weak band at 2.3 μm, none of these bands are evident in the measurements.

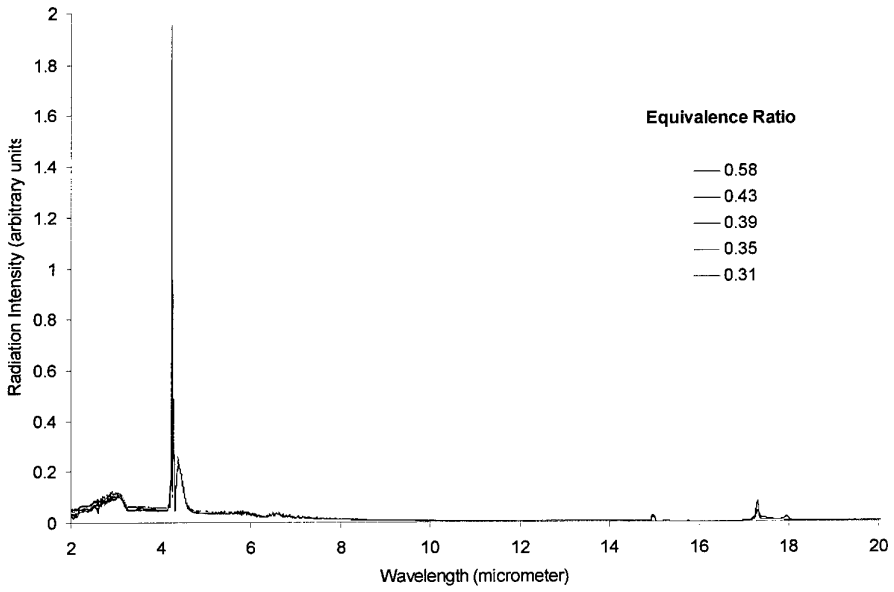

Figure 15: Spectral IR intensity over a waveband 2-20μm, emitted from the cylindrical burner operating at a power density of 139 kW/m² and various equivalence ratios.

The contribution of CO_2 to the radiant intensity is also visible at a wavelength of 2.8 μm. Other significant radiation emission are visible near 2.5μm, 2.7μm, and 2.9μm, which correspond mainly to emission from H_2O molecules. Figure 17, shows the measured IR characteristics in the 2-5μm waveband from the flatbed burner. The intensity distribution is similar to those of the semi-cylindrical burner.

It is worth noting that whilst CO, CO_2 and H_2O all have a well defined principal vibration-rotation bands, the measurements indicate some shift in these bands. For example, H_2O has a fundamental (strong) band at 2.7μm, but the measurements

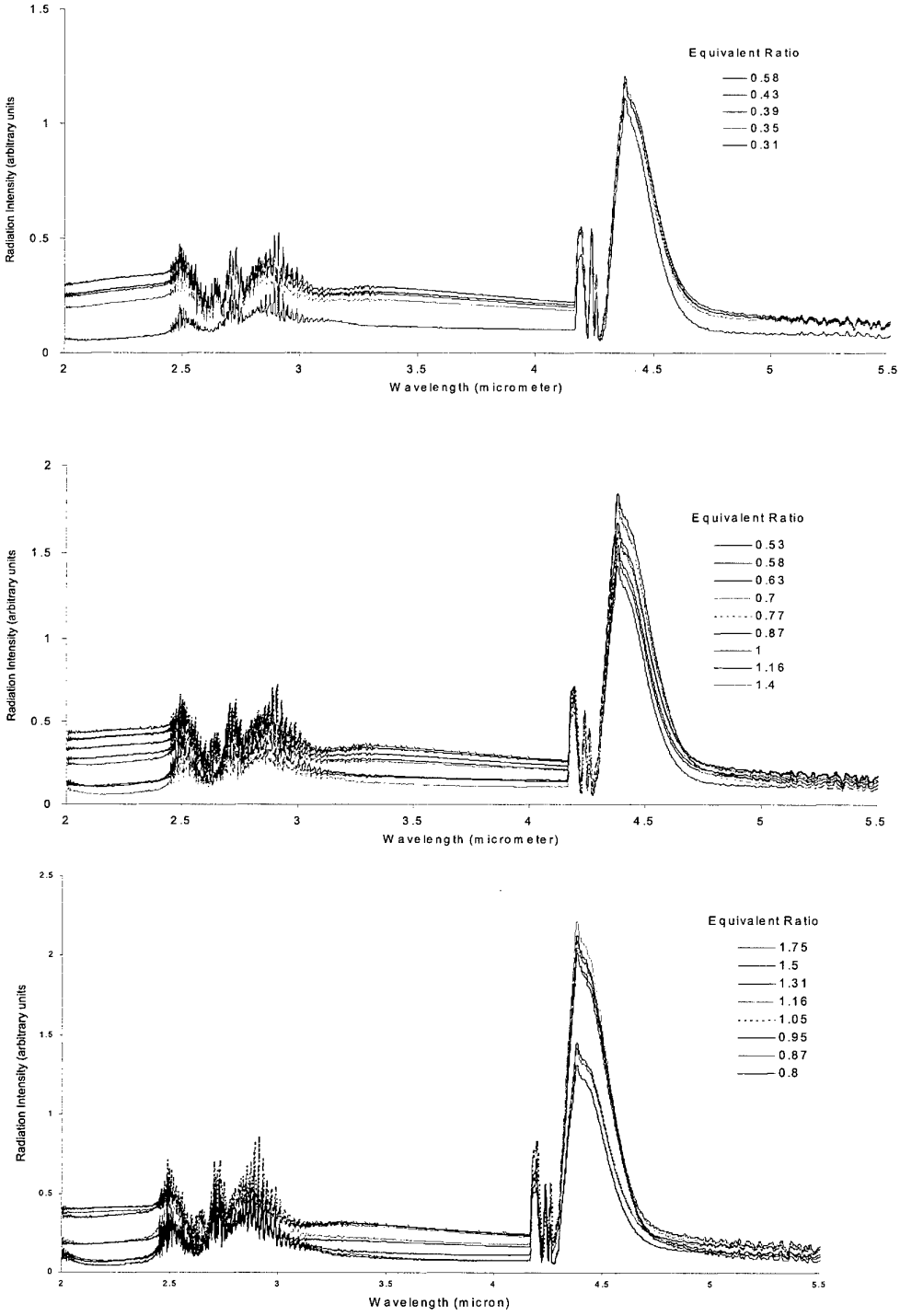

Figure 16: Spectral IR intensity over a waveband 2-5μm, emitted from the semi- cylindrical burner operating at a power density of: (top) 139 kW/m², (middle) 278 kW/m², and (lower) 417 kW/m² , for various equivalence ratios

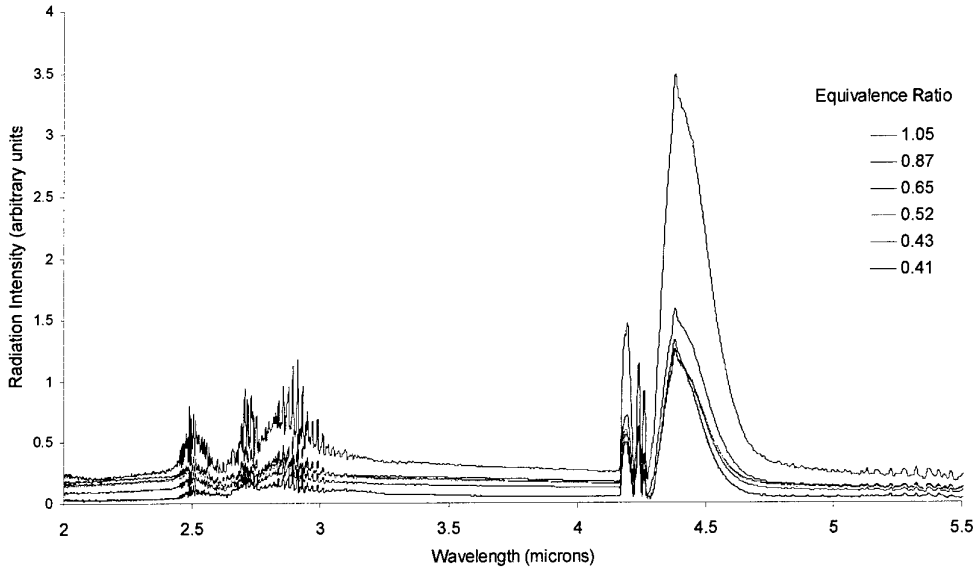

Figure 17: Spectral IR intensity over a waveband 3-5μm, emitted from the flat-bed burner operating at a power density of 63 kW/m², and various equivalence ratios.

show a slight shift of this band to around 2.8μm-2.9μm. There is also a shift in the CO_2 emission from its fundamental band at 4.26μm to a broader band of 4.19μm-4.38μm . These shifts are most likely due to a combined effect of simultaneous molecular absorption-scattering of radiation.

5.2 Numerical Results

Modelling has been performed for a wide range of equivalence ratios and firing rates similar to the experimental conditions. Of particular interest is the semi-cylindrical burner operating at a power density of 417 kW/m², as (experimentally) it provided the most stable flame over a broad range of operating conditions. In all calculations an inlet mixture temperature of 350K has been selected to correspond to that in the experiment.

Whilst, the ChemRad model accounts for 40 species, only major species (in conjunction with the gas and surface temperatures) are presented here to characterise the combustion process. These are CO, CO_2, H_2O, and radical species (*e.g.* OH, O, HO_2 , etc.) which typically are used to identify the location of the flame front. However, in a PRB the flame zone could be relatively thick creating a distributed reaction region. In this region radical species reach their peak concentration though not necessarily at the same physical location as clearly illustrated in Figure 18. Therefore to characterise the flame location in a porous layer, a Reaction-Completion Distance (RCD) term is introduced. It refers to the location at which the fuel conversion is completed. Numerically, the RCD is taken as the location at which the concentration of the fuel drops below 0.1% of its inlet concentration.

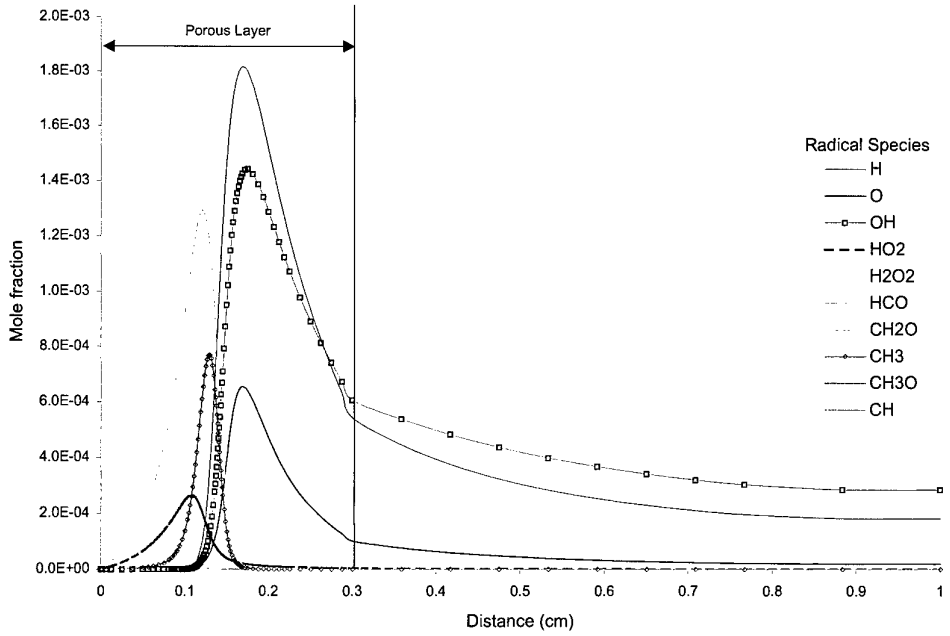

Figure 18: Computed profiles of radical species for a stoichiometric propane-air mixture burning in the semi-cylindrical porous burner (power density of 417 kW/m²).

Figure 19 shows the predicted axial gas temperature profiles for the semi-cylindrical burner (at a power density of 417 kW/m²) at various equivalence ratios. It is clear that for fuel-lean mixtures the gas temperature peaks and levels out within the porous layer. For fuel-rich mixtures, however the temperature peaks near or outside the surface of the burner. This indicates that either the chemical reactions are not fully completed within the porous layer or the flame stabilises entirely above the surface.

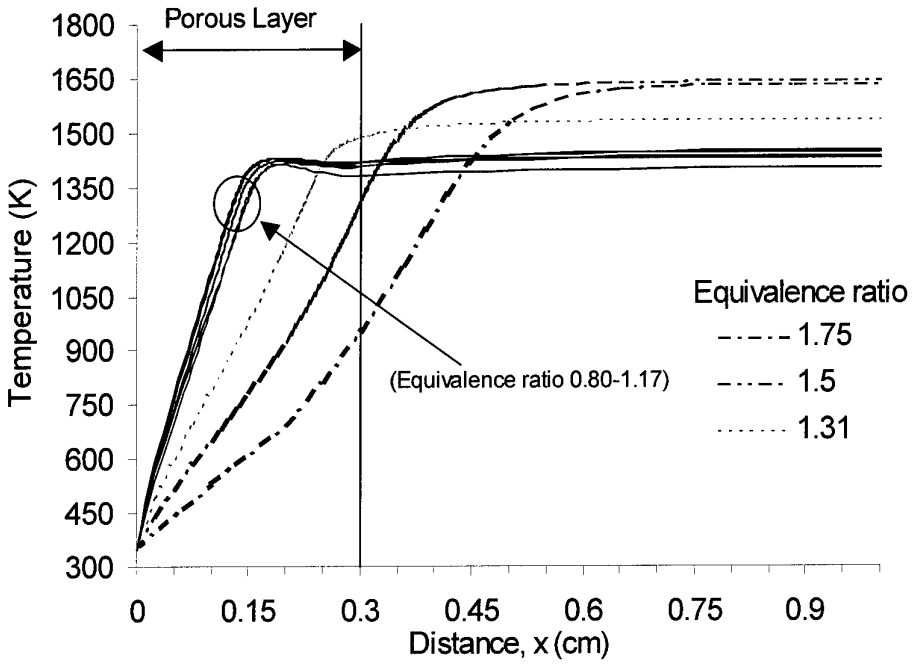

Figure 19: Computed gas temperature distribution of the semi-cylindrical burner for various equivalence ratios (power density of 417 kW/m²) .

Noticeably, in Figure 19 that the temperature profiles of stoichiometric and fuel-lean mixtures (ϕ_c=0.8-1.17) are almost identical. The gas temperature reaches a maximum at the flame front then drops slightly before it stabilises. This drop is attributed to conductive and enhanced radiative heat transfers from the flame zone. However, this behaviour is not evident for fuel-rich mixtures (ϕ_c =1.31, 1.5, and 1.75), as the flame is located outside the porous layer.

The temperature distribution of the wire-mesh within the porous medium (*x=0-0.3 cm*) is shown in Figure 20 only for equivalence ratios ϕ_c =0.8 to 1.17, as the flame is embedded in the porous layer. The figure shows that the solid temperature increases slightly as the equivalence ratio approaches its stoichiometric value. Also shown that the gas temperature at the exit plane is approximately 300K higher than that of the solid temperature.

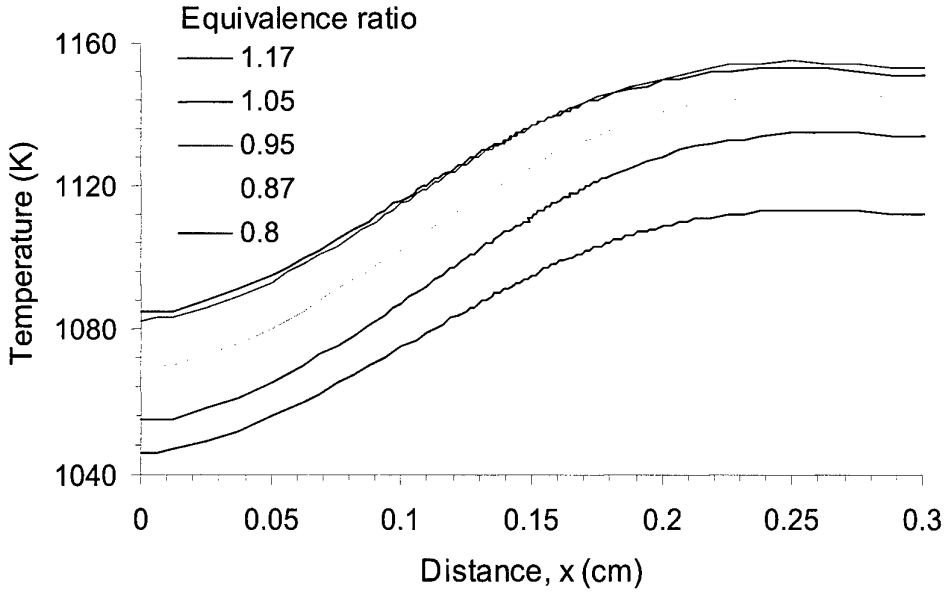

Figure 20: Computed distribution of solid temperature within the wire-mesh of the semi-cylindrical burner for various mixtures (power density of 417 kW/m²).

The dependency of the flame location in term of RCD, on the equivalence ratio is illustrated in Figure 21. The figure shows that for mixtures with an equivalence ratio between 0.8 and 1.3, the flame is fully immersed within the porous layer. Furthermore, for equivalence ratios between 0.8 and 1.15, the flame location is kept almost unchanged, indicating a stable combustion. However, at higher equivalence ratios the location of the flame starts moving towards the surface of the burner and subsequently the flame stabilise above the surface.

The porous layer acts also as a CO-to-CO_2 converter, by which appropriate conditions (temperature, gas velocity, catalytic reactions, etc.) are established causing a conversion of CO into CO_2 before the gases exit the porous medium. Such a low CO level is considered one of the most positive features of PRB technology. The conversion mechanism is illustrated in Figures 22 and 23. The coupling between CO and CO_2 concentrations is particularly evident for mixtures with equivalence ratio between 0.8 and 1.31. Figure 22 shows a clear build-up of CO as the mixture moves from a fuel-lean to fuel-rich. As the equivalence ratio increases the location in which CO peaks, shift towards the exit plane of the burner , and results in a higher CO concentration. The conversion mechanism, however does not exist for fuel-rich mixtures because the flame is located outside the porous medium.

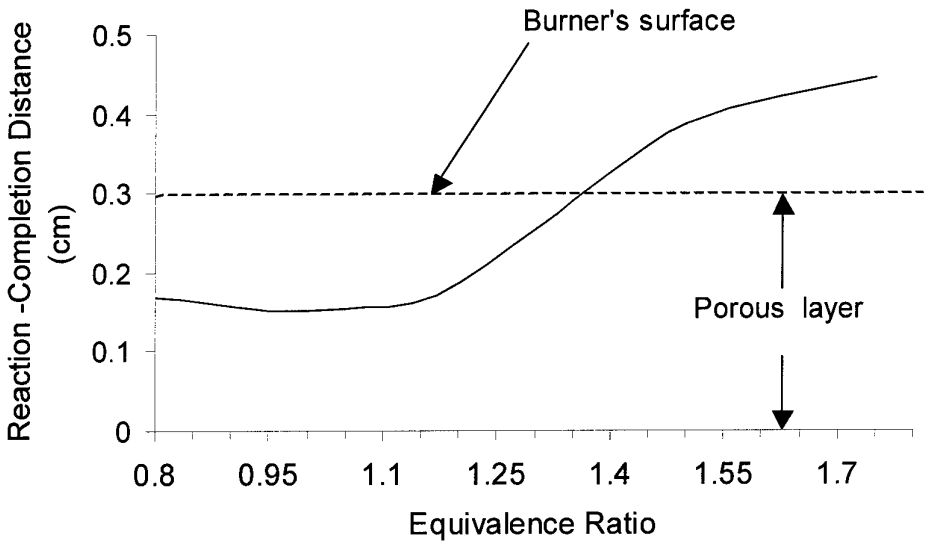

Figure 21: Effect of equivalence ratio on Reaction-Completion Distance.

Another beneficial feature in using PRB technology is its enhanced radiative heat transfer rate. Figure 24 shows the net radiative heat transfer within the solid porous. The results show that as the mixture approaches stoichiometric ratio, the radiation at the surface increases. This is a consistent behaviour with the temperature of the surface, as shown earlier in Figure 20. It should be noted that the radiative heat outside the solid boundaries, ie. in the gas stream, is equal to that at the surface of the burner because the current model treats the gas as a non-participating medium. That is, it does not account for the effects of gaseous product transmission and absorption on the radiation intensity.

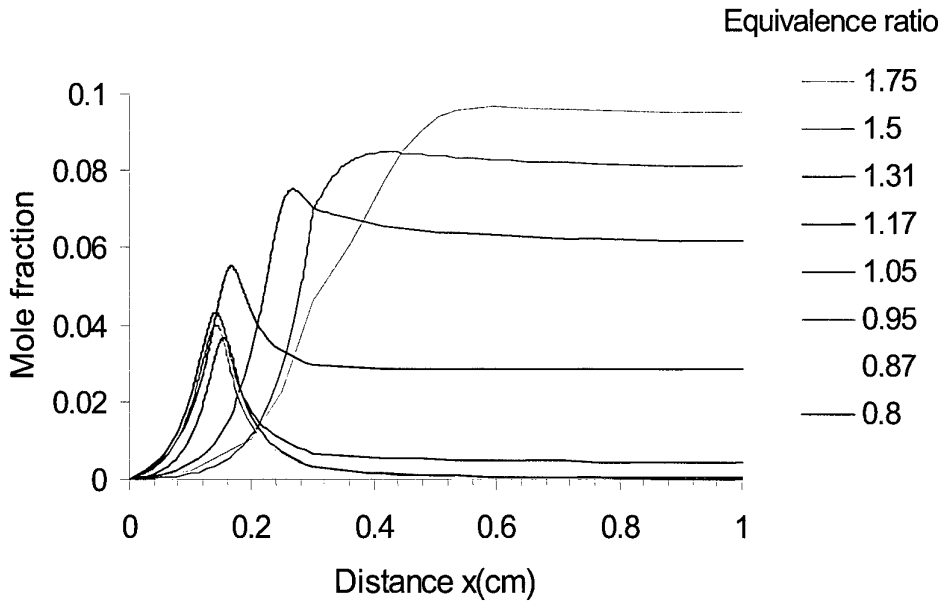

Figure 22: Carbon monoxide (CO) distribution for various mixtures.

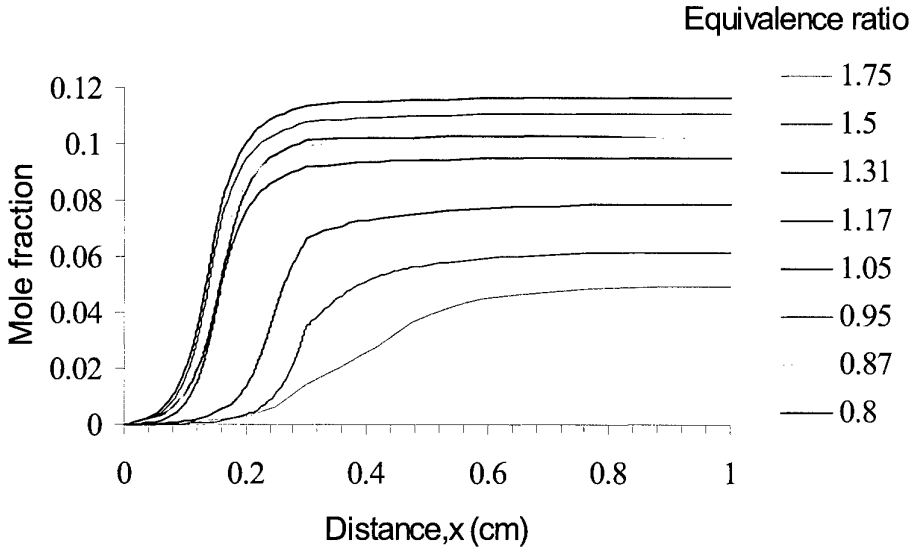

Figure 23: Carbon dioxide (CO_2) profiles for various fuel-to-air mixtures.

Another useful feature of PRB technology is the enhanced radiative heat transfer rates. Radiation efficiency is defined as the ratio between the energy content of the fuel and the radiation energy emitted from the burner's surface. Figure 24 shows the measured radiation efficiency against equivalence ratio for different power densities.

The radiative surface energy is calculated assuming a grey body surface with a 0.8 emissivity, ambient temperature of 300K, and using the measured surface temperature obtained from the MERLIN radiometers (see Table 1). A maximum radiation efficiency of 33% (at ϕ_c=0.77) and 25% (at ϕ_c=0.95) has been measured at firing rates of 278 kW/m^2 and 417 kW/m^2, respectively.

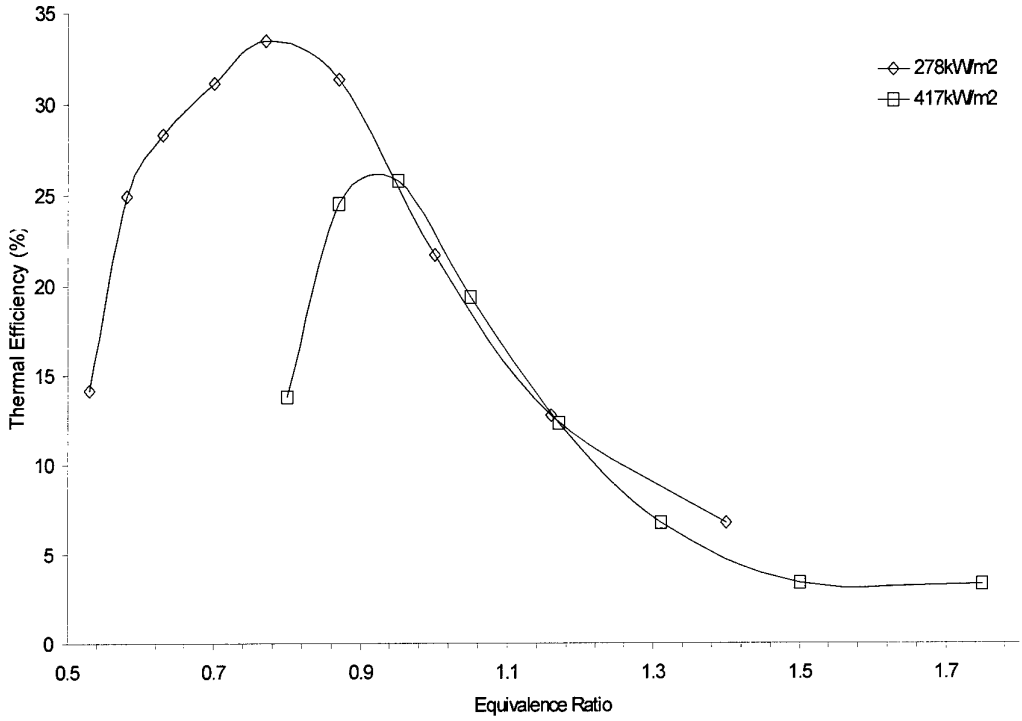

Figure 24: Measured thermal efficiency for various equivalence ratios.

The curves in Figure 24 show the following interesting features; (1) the radiation efficiency decreases as the firing rate increases, and (2) the location in equivalence-ratio space, at which the maximum radiation efficiency is achieved, depends on the firing rate. These results show also that maximum radiation efficiency does not necessarily occur at a stoichiometric mixture. However, increasing the firing rate causes the peak location to shift towards stoichiometry.

5.3 Comparison Between Predictions and Experiment

Because of the grey-body assumption in the radiation model, the only parameter that can be used to compare the PBM predictions with the experimental results is the surface temperature of the burner. Experimentally, the surface temperature has been measured using two independent systems; directly using the MIKRON IR pyrometer and indirectly using the AGEMA images. The results, presented in Figure 25, show similar distribution profiles. However, the temperatures derived from the thermal imager are consistently higher than those obtained by IR pyrometer.

Initially, it was postulated that the discrepancy is related to the assumption of a fixed monochromatic surface emissivity (of 0.8). However an error analysis has shown that the effect of uncertainty in the emissivity on the accuracy, is only a few degrees Celsius. Another possible source of error that has been considered is the effect of the heat shield, in the form of a perspex filter (safety face mask) that was used to reduce the intensity levels from saturation in the thermal imaging system. Even though the surface temperatures were obtained using calibration constants that included the perspex filter characteristics, we noticed non-uniformity in the spectral response. Quantifying the filter effect on the temperature readings however was not possible due to the complex non-linear spectral response of the mask. The discrepancies between the two measurements (relative to the arithmetic mean of both measurements) varies between 4% and 16%, with the maximum discrepancy occurring at an equivalence ratio of 1.31.

A comparison between the model predictions and the mean measured surface temperature shows that the numerical model over-predicts the surface temperature on the fuel-rich region, but under-predicts it on the fuel-lean side of stoichiometry. The discrepancies between the prediction and the measurements are more pronounced in the fuel-rich region. Nevertheless the model shows a similar profile distribution as the experimental profiles.

For fuel-lean mixtures the discrepancies between the model and the experiment varies between 0.1% and 8 %, while for fuel-rich mixture it varies between 8.4% and 16%. There are a number of potential sources that could have contributed to these discrepancies: (1) the high uncertainty in the values of optical properties of the porous media that are used in the model, (2) not including surface (catalytic) reactions, and (3) the model's assumption of adiabatic conditions. However the most likely source of error in the model is the use of a high-temperature kinetics mechanism across the board of equivalence ratios. Figure 25, shows that for equivalence ratios above 1.17, the gas temperature drops below 1000K, which is probably the lower limit for the applicability of high-temperature mechanism. This hypothesis is supported by the experimental results that showed that large discrepancies exist in fuel-rich mixtures, which also correspond to flame with a low temperature. Nevertheless and despite the many simplifying assumptions and uncertainty in a number of parameter values, the model performs reasonably well, both in terms of accuracy and consistency.

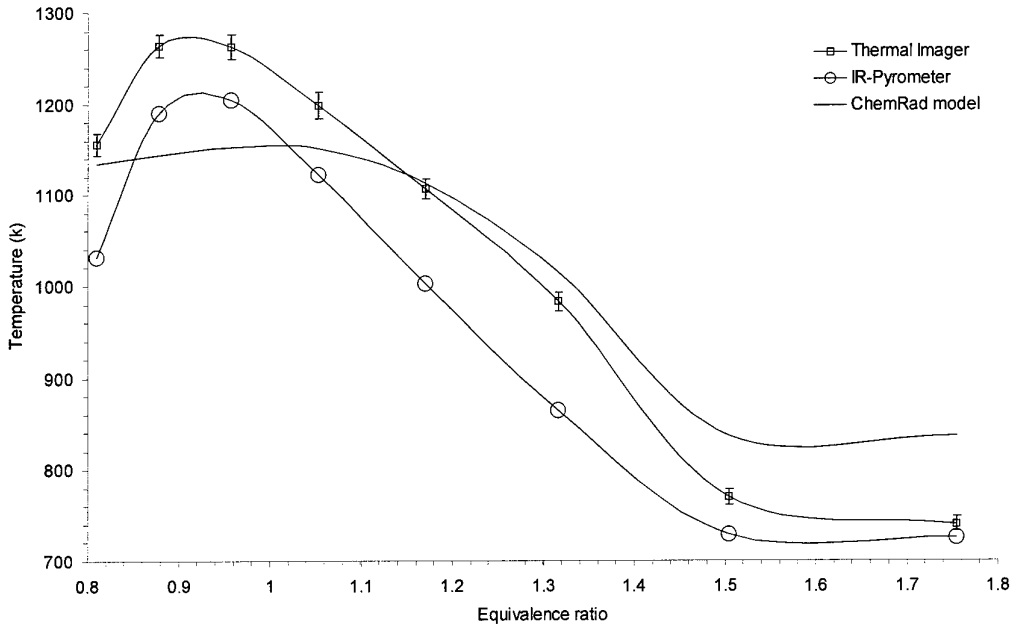

Figure 25: A comparison of the measured and predicted surface temperature of a solid porous medium, for various equivalence ratio mixtures.

5.4 INCONEL601 as a Radiation Shield

The experimental results (see Tables 2 and 3 and Figures 8 –11) have shown that the current PRB configuration does not generate sufficient IR radiation intensity in the 3-5μm waveband to be considered as a potential candidate for air decoys or tracking flares. However, the potential of using the PRB technology as an on-board decoy for platforms, (which require lower temperature/intensity decoys than those used in air systems), is more promising.

The aim is to use PRB technology to reduce or mask the IR signature of naval or land platforms, e.g. masking IR emission of exhaust gases from ships or land vehicles. To investigate the viability of this idea the following experiment has been conducted. A minute amount of approximately *130 mg* of MTV pyrotechnic mixture was pressed in a small cylindrical cup of 8 mm in diameter and 5 mm in height. The MTV mixture was then ignited using a thin layer of primer coated on the surface of the mixture and initiated using a safety match. A small piece of INCONEL601 wire-mesh was placed in front of the MTV cup, as shown schematically in Figure 26, and IR measurements (using the BOMEM FT Spectrometer) were taken for different distances between the wire-mesh and the cup ($D_{c\text{-}m}$).

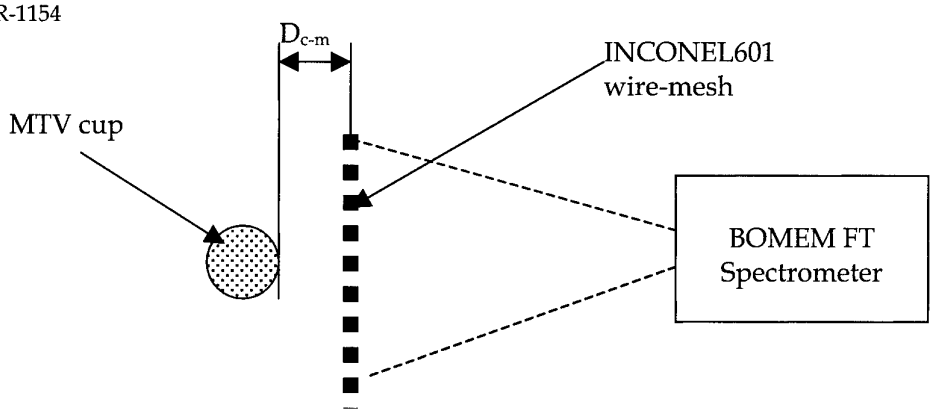

Figure 26: Layout of MTV-Wire-mesh experiment.

The average burn time of the MTV cup was approximately 2 seconds. Initially a bench-mark IR measurement was conducted without the wire-mesh screen. Figure 27, shows the spectral IR intensity as a function of the cup-to-screen distance, and also the reference curve without the screen. It shows that while the screen has no effect on the spectral distribution, it has a profound effect on IR radiation intensity, especially in the 2-2.5 μm range. The closer the screen to the MTV cup is, the higher the reduction in intensity becomes.

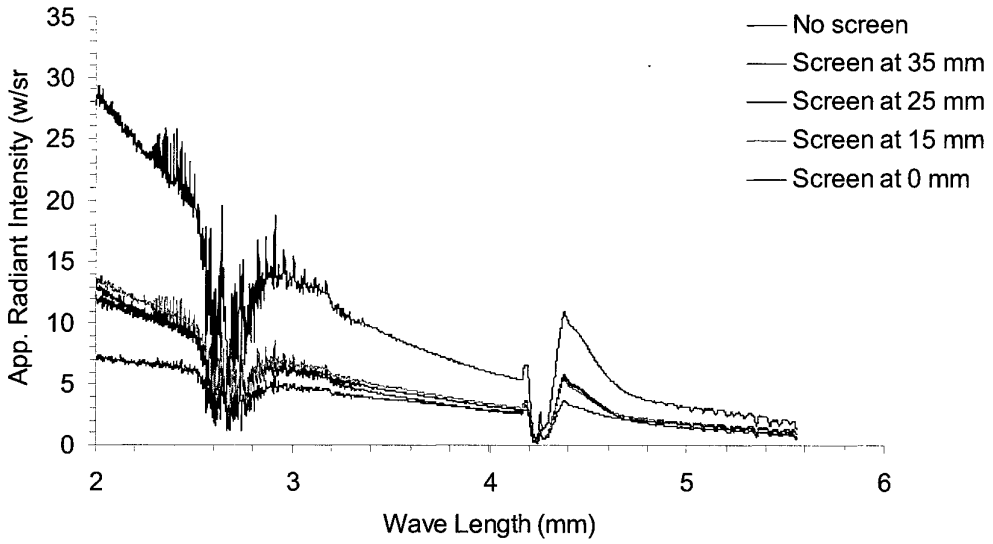

Figure 27: Effect of screen distance from the MTV cup on spectral IR intensity.

The equivalent black-body temperature of the MTV without a screen is ~2170K, however it drops to 1670K when the screen is located adjacent to the MTV cup (D_{c-m}=0). This result indicates that the wire-mesh acts as an effective IR radiation shield. Typically, radiation shields are designed from materials with low emissivity to enhance resistance to radiative transfer. INCONEL601 has a high emissivity (~0.8), nevertheless it still acts as an effective radiation shield. The reason for this behaviour is not yet fully understood. Another advantage for using PRB technique to suppress the IR signature are the lightweight of the wire-mesh structure, possibly low RF signature,

and ease in adaptation to existing platforms. The full potential of such techniques however requires further development and testing using in-service platforms.

6. Concluding Remarks

It has been shown that for an INCONEL601 wire-mesh porous burner, infrared radiation intensity in the 3μm - 5μm waveband is the dominant bandwidth. Within this range only emission spectra of CO_2 and H_2O have been observed. A radiation efficiency of 33% (at ϕ_c=0.77) and 25% ((at ϕ_c=0.95) has been achieved at firing rates of 278 kW/m^2, and 417 kW/m^2 , respectively. The optimal operating conditions of a porous burner, as determined by surface temperature, radiation intensity and efficiency is a function of the fuel-to-air ratio as well as the firing rate. These parameters also influence the location of the flame front. For fuel-rich mixtures the flame front is usually located above the burner's surface, while for lean-fuel mixtures the flame is either embedded in the porous layer or near the surface.

Overall, a reasonable agreement between the predictions and the experimental results has been achieved. This is despite some variability in the measurements, a number of simplifying assumptions and high uncertainty in the values of some physical and optical properties in the model.

The effectiveness of INCONEL601 wire-mesh in suppressing IR signature of MTV pyrotechnics mixture has been successfully demonstrated. This feature gives a rise for new research opportunities into countermeasures for naval and land platforms. However further development is required to fully explore the full potential of such a technique.

7. Acknowledgments

The authors wish to thank Lance Redman, Robert Hall, and Peter Berry for their valuable assistance in operating the instruments. The assistance of Rachel Campbell in scientific photography is also acknowledged.

8. References

1. Christo, F. C., "A Parametric Analysis of a Coupled Chemistry-Radiation Model in Porous Media", DSTO - Research Report RR-0188, 2000.

2. Operating Instruction, " The Porous Radiant Burner Experiment", OI/1 Issue A-AMRL - WSD, February 1999.

3. Fu, X., Viskanta, R., and Gore, J.P., "A Model for the Volumetric Radiation Characteristics of Cellular Ceramics", *Int. Comm. Heat Mass Transfer,* Vol. 24, pp. 1069-1082, 1997.

4. Bouma, P.H., and Goey, L.P.H., " The Stability of Flames on a Ceramic Foam Surface Burner", *Proc. First European Conference on Small Burner Technology and Heating Equipment*, Vol. 1, pp.309-318, Zurich, September 25-26, 1996.

5. Goey, L.P.H., Van de Ven, C.H.J., Bouma P.H., and Drift, A.V.D.," Design of Burner for Combustion in Ceramic Foam", *Proc. First European Conference on Small Burner Technology and Heating Equipment*, Vol. 1, pp.99-108, Zurich, September 25-26, 1996.

Appendix A: Calibration and Analysis for BOMEM MR254 Spectrometer

In order to calibrate the spectrometer, a blackbody radiator (calibrated to National Standards at the National Measurement Laboratory, Lindfield, NSW) is placed immediately in front of the spectrometer aperture in order to flood fill the device. Measurements are taken in this arrangement for two different blackbody temperatures. The theoretical radiance is given by:

$$L_U(\nu) = \frac{c_1 \nu^3}{\pi\left(e^{\frac{c_2 \nu}{T_U}} - 1\right)} \qquad \text{A(1)}$$

$$L_L(\nu) = \frac{c_1 \nu^3}{\pi\left(e^{\frac{c_2 \nu}{T_L}} - 1\right)} \qquad \text{A(2)}$$

where:

$L_U(\nu)$ is the theoretical blackbody radiance for the upper temperature,
$L_L(\nu)$ is the theoretical blackbody radiance for the lower temperature,
ν is the wavenumber in units of cm^{-1},
T_U, T_L are the upper and lower temperatures respectively and
C_1, C_2 are the first and second radiation constants:
$C_1 = 3.7415 \times 10^{-12}$ $[W/cm^2/cm^{-1}]$
$C_2 = 1.43879$ [cm K].

The spectrometer signal is given by:

$$V(\nu) = G(\nu)L(\nu) + O(\nu) \qquad \text{A(3)}$$

where:

V(ν) is the spectrometer voltage output,
G(ν) is the instrument gain and
O(ν) is the instrument offset.

Hence the instrument gain and offset are determined as follows:

$$G(\nu) = \frac{V_U(\nu) - V_L(\nu)}{L_U(\nu) - L_L(\nu)} \qquad \text{A(4)}$$

$$O(\nu) = V_U(\nu) - G(\nu)L_U(\nu) = V_L(\nu) - G(\nu)L_L(\nu) \qquad \text{A(5)}$$

All subsequent measurements are converted from voltage output to radiance using the following relation:

$$L(\nu) = \frac{V(\nu) - O(\nu)}{G(\nu)} \qquad \text{A(6)}$$

The radiance measurement can then be converted to apparent radiant intensity or irradiance as desired:

$$I(\nu) = L(\nu) A_S \qquad \text{A(7)}$$

$$E(\nu) = \frac{L(\nu) A_S}{d^2} \qquad \text{A(8)}$$

where:

I(ν) is the apparent radiant intensity observed,
E(ν) is the irradiance observed,
A_S is the projected area of view of the telescope used at the range of the target, and
d is the distance between the source and the spectrometer.

Appendix B: Calibration and Analysis Methodology for Thermal Imager Data

Calibration

The thermal imagers are calibrated at the Agema manufacturing facility by observing a series of large aperture blackbody radiators at various temperatures. The imager forms a focussed image of the blackbody that has sufficient extent as to occupy at least 10 adjacent pixels. The output of the imager (Λ) in digital levels(*dl*) is due to the convolution of its spectral response function with the spectral radiance of the blackbody at the set temperature:

$$\Lambda = \int L(T,\lambda.)\phi(\lambda)d\lambda$$

$$\Lambda = \frac{\int M(T,\lambda.)\phi(\lambda)d\lambda}{\pi} \qquad \text{B(1)}$$

By measuring a range of temperatures, a set of output values as a function of apparent effective radiance can be obtained. It is found that this function is approximately linear and that the calibration function can be represented as a linear polynomial:

$$\Lambda = k.\int L(T,\lambda).\phi(\lambda).\tau(\lambda)d\lambda \qquad \text{B(2)}$$

The calibration constants for the two aperture settings used on the Agema 900 thermal imager were 0.38 μWcm^2/sr/pixel/*dl* and 1.4 μWcm2/sr/pixel/*dl*. These have been verified by calibration checks performed in the laboratory.

Analysis

The calibration constant was used in this analysis to convert the output values of each pixel from the imager into the effective apparent radiance. The measured apparent radiance is the sum of the radiance due to the target source and the path radiance due to emissions from the atmosphere. The background radiance, at the ranges involved in these measurements, has been found to closely approximate the path radiance. The radiance due to the target source alone can therefore be found by subtracting the background radiance (= path radiance) from the measured radiance:

$$\begin{aligned} L_{SWB} &= \int L(T,\lambda).\phi_{SWB}(\lambda).\tau(\lambda)d\lambda \\ &= \int Lmeas(T,\lambda).\phi(\lambda)d\lambda - \int Lpath(T,\lambda.)\phi(\lambda).\tau(\lambda)d\lambda \end{aligned} \qquad \text{B(3)}$$

This quantity is referred to as the apparent effective radiance corrected for path radiance. Note that the effect of absorption by the intervening atmosphere is not removed in this analysis.

The apparent effective radiant intensity of the source is calculated by multiplying the projected area of a pixel by the corrected apparent effective radiance detected by each pixel:

$$I_{SWB} = a.\sum_{i}^{n_p}(L_{SWB})_i \qquad \text{B(4)}$$

$$= \Omega.d^2.\sum_{i}^{n_p}(L_{SWB})_i$$

where a = projected area of one pixel
n_p = number of pixels containing target source
Ω = solid angle for one pixel (= 10^{-7} sr for FOV of 5 degrees).
d = distance between target source and sensor.

DISTRIBUTION LIST

Experimental and Numerical Analysis of Thermal Radiation from a Porous Radiant Burner

Farid C. Christo and Lakshmanan V. Krishnamoorthy

AUSTRALIA

DEFENCE ORGANISATION

Task Sponsor **DGAD**

S&T Program

Chief Defence Scientist
FAS Science Policy
AS Science Corporate Management
Director General Science Policy Development
} shared copy

Counsellor Defence Science, London (Doc Data Sheet)
Counsellor Defence Science, Washington (Doc Data Sheet)
Scientific Adviser to MRDC Thailand (Doc Data Sheet)
Scientific Adviser Policy and Command
Navy Scientific Adviser (Doc Data Sheet and distribution list only)
Scientific Adviser - Army (Doc Data Sheet and distribution list only)
Air Force Scientific Adviser
Director Trials

Aeronautical and Maritime Research Laboratory
Director

Chief of Weapons Systems Division
Research Leaders (WSD), RLAWS, and RLJI
Head Pyrotechnics, WSD
Head Terminal Effects, WSD
Head Propulsion Systems Technology, WSD
Dr. L. Krishnamoorthy, WSD
Dr. F. Christo, WSD
Dr. N. Smith, AED

DSTO Library and Archives
Library Fishermans Bend (Doc Data Sheet)
Library Maribyrnong (Doc Data Sheet)
Library Salisbury
Australian Archives
Library, MOD, Pyrmont (Doc Data sheet only)
US Defense Technical Information Center, 2 copies
UK Defence Research Information Centre, 2 copies
Canada Defence Scientific Information Service, 1 copy
NZ Defence Information Centre, 1 copy
National Library of Australia, 1 copy

Capability Systems Staff

Director General Maritime Development (Doc Data Sheet only)
Director General Land Development
Director General Aerospace Development (Doc Data Sheet only)

Knowledge Staff

Director General Command, Control, Communications and Computers (DGC4) (Doc Data Sheet only)
Director General Intelligence, Surveillance, Reconnaissance, and Electronic Warfare (DGISREW)R1-3-A142 CANBERRA ACT 2600 (Doc Data Sheet only)
Director General Defence Knowledge Improvement Team (DGDKNIT) R1-5-A165, CANBERRA ACT 2600 (Doc Data Sheet only)

Army

Stuart Schnaars, ABCA Standardisation Officer, Tobruck Barracks, Puckapunyal, 3662(4 copies)
SO (Science), Deployable Joint Force Headquarters (DJFHQ) (L), MILPO Gallipoli Barracks, Enoggera QLD 4052 (Doc Data Sheet only)
NPOC QWG Engineer NBCD Combat Development Wing, Tobruk Barracks, Puckapunyal, 3662 (Doc Data Sheet relating to NBCD matters only)

Air Force

DDEW
Pyrotechnics and countermeasures Group, JALO, Defence Establishment, Orchard Hills, NSW.

Intelligence Program

DGSTA Defence Intelligence Organisation
Manager, Information Centre, Defence Intelligence Organisation

Corporate Support Program

Library Manager DLS-Canberra

UNIVERSITIES AND COLLEGES

Australian Defence Force Academy
Library
Head of Aerospace and Mechanical Engineering
Serials Section (M list), Deakin University Library, Geelong, 3217
Hargrave Library, Monash University (Doc Data Sheet only)
Librarian, Flinders University

OTHER ORGANISATIONS

NASA (Canberra)
AusInfo

OUTSIDE AUSTRALIA

ABSTRACTING AND INFORMATION ORGANISATIONS

Library, Chemical Abstracts Reference Service
Engineering Societies Library, US
Materials Information, Cambridge Scientific Abstracts, US
Documents Librarian, The Center for Research Libraries, US

INFORMATION EXCHANGE AGREEMENT PARTNERS

Acquisitions Unit, Science Reference and Information Service, UK
Library - Exchange Desk, National Institute of Standards and Technology, US
National Aerospace Laboratory, Japan
National Aerospace Laboratory, Netherlands

SPARES (5 copies)

Total number of copies: 53

DEFENCE SCIENCE AND TECHNOLOGY ORGANISATION
DOCUMENT CONTROL DATA

1. PRIVACY MARKING/CAVEAT (OF DOCUMENT)

2. TITLE

An Experimental and Numerical Study of IR Emission from a Porous Radiant Burner

3. SECURITY CLASSIFICATION (FOR UNCLASSIFIED REPORTS THAT ARE LIMITED RELEASE USE (L) NEXT TO DOCUMENT CLASSIFICATION)

Document	(U)
Title	(U)
Abstract	(U)

4. AUTHOR(S)

Farid C. Christo and Lakshmanan V. Krishnamoorthy

5. CORPORATE AUTHOR

Aeronautical and Maritime Research Laboratory
506 Lorimer St
Fishermans Bend Vic 3207 Australia

6a. DSTO NUMBER	6b. AR NUMBER	6c. TYPE OF REPORT	7. DOCUMENT DATE
DSTO-TR-1154	AR-011-870	Technical Report	May 2001

8. FILE NUMBER	9. TASK NUMBER	10. TASK SPONSOR	11. NO. OF PAGES	12. NO. OF REFERENCES
J 9505-19-106-1	AIR 98/116	DGAD	32	5

13. URL on the World Wide Web

http://www.dsto.defence.gov.au/corporate/reports/DSTO-TR-1154.pdf

14. RELEASE AUTHORITY

Chief, Weapons Systems Division

15. SECONDARY RELEASE STATEMENT OF THIS DOCUMENT

Approved for public release

OVERSEAS ENQUIRIES OUTSIDE STATED LIMITATIONS SHOULD BE REFERRED THROUGH DOCUMENT EXCHANGE, PO BOX 1500, SALISBURY, SA 5108

16. DELIBERATE ANNOUNCEMENT

No Limitations

17. CASUAL ANNOUNCEMENT Yes

18. DEFTEST DESCRIPTORS

combustion, modelling, infrared, porous medium, MTV

19. ABSTRACT

An experimental analysis and computational modelling of thermal radiation from an INCONEL601 wire-mesh porous burner has been conducted. It has been found that within a bandwidth between 2μm and 20μm, the infrared radiation in the 2-5μm waveband is the dominant band. Optimal operating conditions, as determined by the surface temperature and radiant intensity, are a function of the equivalence ratio and the firing rate. The location of the flame front is also influenced by these parameters. For fuel-rich mixtures the flame is usually located above the surface and the flame stability is sensitive to external perturbations. A maximum surface temperature of approximately 1223K, and a radiation intensity of 50 W/Sr, has been measured. It has also been shown that INCONEL601, despite its high emissivity, can be used as an effective radiation shield. By placing a piece of the wire-mesh in front of burning MTV pyrotechnic composition, the infrared radiation was significantly reduced. The equivalent black body temperature of MTV was cut from ~1900°C without a shield to ~1400°C with a shield adjacent to the mixture.

A comparison between the ChemRad model predictions and measured surface temperature for various equivalence ratios has shown a reasonable agreement with a maximum discrepancy of 16% for fuel-rich mixtures. However, within optimal operating conditions of the burner (equivalence ratio 0.8- 1) a maximum difference of 8% has been observed. Accounting for the variability in the measurements, the number of simplifying assumptions and the uncertainty in some values of the physical and optical properties, the accuracy and consistency of the model, as a first-order approximation is acceptable.

DEPARTMENT OF DEFENCE DSTO
DEFENCE SCIENCE & TECHNOLOGY ORGANISATION
AERONAUTICAL AND MARITIME RESEARCH LABORATORY
506 LORIMER STREET FISHERMANS BEND VICTORIA 3207 AUSTRALIA
TELEPHONE (03) 9626 7000